Multidirectional Flow Apparatus for Assessing Soil Internal Erosion Susceptibility

Didier Marot, Dinh Minh Tran, Fateh Bendahmane, van Thao Le

Marot D., Tran D.M., Bendahmane F., Le V.T. (2020). Multi-directional flow apparatus for assessing soil internal erosion susceptibility. Geotechnical Testing Journal, 43(6), pp 1481-1498, doi:10.1520/GTJ20190254

Multi-directional Flow Apparatus for Assessing Soil Internal Erosion Susceptibility

Didier MAROT[1], Dinh Minh TRAN[2], Fateh BENDAHMANE[3], Van Thao LE[4]

[1] Prof. Didier Marot
Institut de Recherche en Génie Civil et Mécanique, Université de Nantes
58 rue Michel Angle, BP 420
F-44606 Saint - Nazaire cedex, France
Email: didier.marot@univ-nantes.fr

[2] Dinh Minh TRAN
Institut de Recherche en Génie Civil et Mécanique, Université de Nantes
58 rue Michel Angle, BP 420
F-44606 Saint - Nazaire cedex, France
The University of Danang -University of Science and Technology
54, Nguyen Luong Bang, Da Nang, Vietnam
Email: dinh-minh.tran@etu.univ-nantes.fr

[3] Dr. Fateh BENDAHMANE
Institut de Recherche en Génie Civil et Mécanique, Université de Nantes
58 rue Michel Angle, BP 420
F-44606 Saint - Nazaire cedex, France
Email: fateh.bendahmane@univ-nantes.fr

[4] Van Thao LE
Institut de Recherche en Génie Civil et Mécanique, Université de Nantes
58 rue Michel Angle, BP 420
F-44606 Saint - Nazaire cedex, France
The University of Danang -University of Science and Technology
54, Nguyen Luong Bang, Da Nang, Vietnam
Email: lvthao@dut.udn.vn

Corresponding author: Didier Marot
Tel: 33 2 40 17 81 91
didier.marot@univ-nantes.fr

ABSTRACT

Suffusion is a selective erosion of fine particles within the matrix of coarse soil particles under the effect of seepage flow. Suffusion can induce important modifications in the hydraulic and mechanical characteristics of the soil. At the scale of an earth structure, the flow direction can vary and the soils which compose the structure and its foundations can be heterogeneous. Thus to ensure the safety assessment of hydraulic earth structures, the suffusion tests need to match with the reality of the body of dikes or dams with a possible horizontal or vertical flow and heterogeneous soils. In this paper, a new multi-directional flow apparatus was developed for characterizing soil susceptibility facing suffusion process and to study the effect of flow direction. The apparatus allows the specimen tests under a vertical or a horizontal flow and it permits to select the layer in which the flow is injected. Two cohesionless soils which slightly differ from each other in their gradations were used to prepare eight specimens by compaction per layer. Suffusion tests were performed under multi-stage hydraulic gradient and the suffusion susceptibility was evaluated by the energy based method. In the case of specimens composed by one soil, whatever the flow direction compared to the interface between soil layers, tested soils appear slightly more erodible under vertical downward flow. These results highlight the combination effect of the hydraulic loading and the gravity on the detached particles. In the case of specimens constituted by a layer of each tested soil, the results show that under a perpendicular flow to the interface between soil layers, the suffusion susceptibility is mainly influenced by the more resistant soil. But conversely, in the case of a parallel flow to the interface between both soils, the suffusion susceptibility is mostly influenced by the less resistant soil.

Keywords Internal erosion, laboratory testing, flow direction, suffusion, susceptibility classification.

Introduction

Internal erosion is one of the main causes of instabilities within hydraulic earth structures such as dams, dikes or levees (Foster et al. 2000). According to Fell and Fry (2013), there are four types of internal erosion: concentrated leak erosion, backward erosion, contact erosion and suffusion. This paper focuses on suffusion which is a selective erosion of fine particles under the effect of seepage flow within the matrix of coarser particles. It is recognized that suffusion may cause changes in porosity and can also lead to important modifications in the hydraulic and mechanical characteristics of the soil (Marot et al. 2009, Chang and Zhang 2011; Ke and Takahashi 2012; Moffat et al. 2011 among others). Moreover, modifications of the porous medium can be the catalyst for slope instability at the scale of hydraulic embankments (Fry et al. 2012). Thus, to ensure the safety assessment of hydraulic earth structures, suffusion susceptibility must be characterized.

For the characterization of suffusion occurrence, Fell and Fry (2013) proposed three criteria that have to be satisfied. The first criterion concerns the geometry of the porous media and points out that the size of the constrictions between the coarser particles must be larger than the size of detached particles. The second criterion is related to the stress applied on the fine fraction and the third one takes into account the hydraulic load. The two first criteria are mainly related to the grain size distribution, and proposals of various geometric assessment methods exist in the literature, mostly based on the particle size distribution (Kenney and Lau 1985; Wan and Fell 2008; Chang and Zhang 2013, among others). However, the modification of the effective stress can also influence the suffusion susceptibility (Moffat and Fannin 2006; Bendahmane et al. 2008; Chang and Zhang 2011). Finally, for a given grain size distribution and a given value of effective stress, angularity of coarse fraction grains contributes to increase the suffusion resistance (Marot et al. 2012). The third criterion is related to the

action of the fluid phase, i.e., to the seepage loading required to detach and then to transport the fine particles. Fell and Fry (2013) proposed to model this loading by the velocity of flow through the soil matrix. However, the suffusion development can also be accompanied by variations of interstitial pressure (Moffat and Fannin 2006, Sail et al. 2011). In this context and further to results on interface erosion tests, Marot et al. (2011a) proposed an analysis based on the total flow power which is the summation of the power transferred from the fluid to the solid particles and the power dissipated by the viscous stresses in the bulk. According to Sibille et al. (2015), the transfer appears negligible in the case of suffusion and the authors suggested characterizing the fluid loading from the total flow power (expressed in W) which is computed by:

$$P_{flow} = \left(\gamma_w \Delta z + \Delta P\right) \; Q \tag{1}$$

where Q is the fluid flow rate (in $m^3\ s^{-1}$), γ_w is the specific weight of water (in $N\ m^{-3}$), $\Delta P = P_A - P_B$ is the pressure drop (in Pa) between the upstream section A and the downstream section B, $\Delta z = z_A - z_B$, z_A and z_B are altitudes (in m) of sections A and B respectively. $\Delta z > 0$ if the flow is in downward direction, $\Delta z < 0$ if the flow is upward and the total flow power is equal to $Q\ \Delta P$ if the flow is horizontal.

The expended energy E_{flow} (expressed in J) is the time integration of the instantaneous power dissipated by the water seepage and it is computed until reaching the steady state (i.e., hydraulic conductivity tends to stabilize and the erosion rate tends to decrease). Hence the expended energy is expressed by:

$$E_{flow} = \int_0^{t_f} P_{flow}(t)\,\mathrm{d}t \tag{2}$$

where t_f is the time (in s) corresponding to the stabilization of the hydraulic conductivity and the decrease of the erosion rate.

For the same duration, the cumulative eroded dry mass is determined (expressed in kg) and the erosion resistance index is expressed by:

$$I_\alpha = -\log\left(\frac{Cumulative\ \ eroded\ \ dry\ \ mass}{E_{flow}}\right) \quad (3)$$

Depending on the values of I_α index, Marot et al. (2016) proposed six categories of suffusion susceptibility from highly erodible to highly resistant (corresponding susceptibility categories: highly erodible for $I_\alpha < 2$; erodible for $2 \le I_\alpha < 3$; moderately erodible for $3 \le I_\alpha < 4$; moderately resistant for $4 \le I_\alpha < 5$; resistant for $5 \le I_\alpha < 6$; and highly resistant for $I_\alpha \ge 6$). This suffusion susceptibility chart brings a more sensitive characterization of the erodibility compared to grain size based criteria which only distinguish two types of gradation: stable or unstable. Moreover it is complementary to the charts defined for the other erosion processes. These include the charts proposed by Briaud (2008) based on erosion tests performed with Erosion Function Apparatus, by Hanson and Simon (2001) and by Wan and Fell (2004) for Jet Erosion Test and Hole Erosion Test, respectively, and by Marot et al. (2011a) for both Jet Erosion Test and Hole Erosion Test.

For characterizing the initiation and development of this complex internal erosion process, experimental devices comprise a rigid wall permeameter (Kenney and Lau 1985; Skempton and Brogan 1994; Moffat and Fannin 2006; Wan and Fell 2008; Sail et al. 2011) or a modified triaxial cell designed to force fluid to percolate throughout the sample (Bendahmane et al. 2008; Marot et al. 2009; Chang and Zhang 2011; Ke and Takahashi 2014; Slangen and Fannin 2017). These laboratory devices permit to apply a vertical flow in upward or downward direction. However, the suffusion process could be influenced by the flow direction, which can be completely different from vertical flow direction in situ. Pachideh and Mir Mohammad Hosseini (2019) developed a new apparatus to study the effect of the

flow direction on the suffusion susceptibility of compacted specimens. They distinguished three types of hydraulic gradients: (i) threshold, (ii) occurrence and (iii) development. These gradients are defined by the start of: rotational movement of fine particles, formation of micropipes and creation of pipes. Pachideh and Mir Mohammad Hosseini concluded that the bigger the angle between the flow direction and the gravity axis, the more these gradients increase. However, the visual detection of such gradients is not easy and in addition, Rochim et al. (2017) showed that the history of hydraulic loading can substantially modify the value of the critical hydraulic gradient at which suffusion occurs. Finally, Smith and Konrad (2011) showed that the soil fabric has an influence on the hydraulic conductivity of compacted soil which suggests the interest of the suffusion susceptibility characterization on undisturbed specimens.

In this context, the main objective of this research is to develop a multidirectional flow apparatus which can be used to study soil suffusion susceptibility of undisturbed or compacted specimens. The device also gives the opportunity to apply vertical or horizontal flows and parallel or perpendicular ones with interface between two layers of soils.

Testing Apparatus

The general configuration of the testing apparatus is shown in Fig. 1. It is composed of an acrylic cylinder cell, a system for applying axial stress, a soil collection system, a water supply system, instrumentation and a data acquisition system.

CYLINDER CELL

This device has been developed to perform suffusion test directly in the cell of the core sample. Such cells have an acrylic cylinder form with an inner diameter of 80 mm and its height can reach up to

500 mm. The device gives the possibility to test specimen with various heights between 300 mm and 400 mm. The methodology which is defined by the Patent (2018) permits to avoid pushing the sample out of the cell and so limits the soil disturbances. However for this study, in order to reach the same order of magnitude of density for all tested specimens, soils were compacted per layers in the cell of core sampler (see Fig. 1). For applying a vertical flow along the specimen length, the cell is vertically fixed by two vertical beams with two clamps to avoid any disturbances. Two configurations can be used in order to apply a horizontal flow: (i) the cell can be placed horizontally and the seepage flow percolates along the specimen length (configuration named horizontal #1 flow), (ii) the cell can be vertical and a horizontal flow can be injected along the specimen's diameter. For this second configuration, the horizontal flow (named horizontal #2 flow) is injected through an inlet and outlet ports fixed on the vertical beams. For the three possible test configurations, the letters A and B show in Fig. 1 the positions of upstream and downstream sections, respectively (in detail: Av and Bv for vertical flow, Ah#1 and Bh#1 for horizontal #1 flow and finally, Ah#2 and Bh#2 for horizontal #2 flow). Figure 2 shows the different parts, identical in form for both inlet #2 and outlet #2. In the buffer zone of inlet #2, a 15 mm thick layer of glass beads is introduced to diffuse the fluid. The pedestal base (the corresponding section is named Bv for vertical flow and Bh#1 for horizontal #1 flow) and the horizontal outlet #2 are specially designed to perform suffusion tests i.e., to catch the detached particles and also to act as a downstream filter. The specimen is positioned on a 10 mm opening size grid (see Fig. 3) and a mesh with a selected pore opening size can come in between. The inner diameter of the outlet #2 is 10 mm (see Fig. 2) and a same type of aforementioned mesh is fixed on the opening. The vertical funnel-shaped draining system and the horizontal outlet #2 are both connected to an effluent tank by a pipe having a glass portion. Figure 4 shows the cell's upstream end (the corresponding section is named Av

for vertical flow and Ah#1 for horizontal #1 flow) which is closed by a cap equipped with an inlet port, an opening for the passage of the axial load ram and a vent. For the measurement of the gradient of interstitial pressure, the cell is equipped with four pressure ports: at the horizontal inlet and outlet #2 (see Fig. 2), the base pedestal (see Fig. 3) and the top cap (see Fig. 4).

AXIAL LOADING SYSTEM

The loading system is used to apply axial stress on both vertical and horizontal specimens, through a pneumatic piston (see Fig. 4) which can move up or down. This piston contains a 15 mm thick layer of glass beads to diffuse the fluid uniformly on the specimen top surface. The air pressure system is controlled by using a valve and a dial gauge displays the value of air pressure from 0 to 12 bars.

SOIL COLLECTION SYSTEM

The effluent tank is equipped with three inlet valves and an overflow outlet to control the downstream hydraulic head (see Fig. 5). Two inlets permit to collect the effluent for flow applied along the specimen length or along the specimen diameter. The third inlet is connected to the upstream reservoir in order to saturate the specimen by an upward flow (see Fig. 1). Within the effluent tank, a rotating system contains 8 beakers with eight linen bags for the sampling of eroded particles carried with the effluent. In the case of clay or silt suffusion, a multi-channel optical sensor can be placed around the glass pipe (Marot et al. 2011b).

WATER SUPPLY SYSTEM

As suffusion is the result of the combination of three processes: detachment, transport and filtration, which in particular depends on the history of hydraulic loading, Rochim et al. (2017) recommend performing suffusion test under multistage hydraulic gradient. For this purpose, the water supply system includes upstream and downstream reservoirs both equipped with an overflow and their

relative elevation that can be manually modified. By taking into account the difference of hydraulic head between the free water surfaces in upstream and downstream reservoirs, the range of hydraulic gradient is from 0 to 2.6 for a vertical flow through a 400 mm high specimen and up to 13 for a flow along the specimen diameter.

INSTRUMENTATION AND DATA ACQUISITION SYSTEM

The instrumentation includes: two flow meters, a differential pressure transducer, an optical sensor and a mass balance as shown in Fig. 1. The injected seepage flow is measured with two electromagnetic flowmeters (of different capacities 0.05-2 L/min and 2-40 L/min) located between the upstream reservoir and injection inlets. The corresponding accuracy is ± 1.5% of the full scale. Depending on the hydraulic conductivity of soils, a set of gates permits to select the appropriate flow meter. In case of very low hydraulic conductivity, at the overflow outlet of the effluent tank, water falls in a beaker which is continuously weighed in order to determine injected flow rate with a precision ± 0.01 $cm^3.s^{-1}$. The same differential pressure transducer (pressure range of -50 kPa to 50 kPa, accuracy of ± 0.01%) is used for horizontal or vertical flows. For vertical flow or for horizontal #1 flow, the differential pressure transducer is connected to the pressure ports of the top cap and the pedestal base. For horizontal #2 flow, it is connected to the pressure ports of horizontal inlet and outlet. The accuracy of hydraulic gradient measurement for flow along the specimen length and the specimen diameter is 0.01 and 0.17, respectively. Thanks to a previous calibration, the optical sensor allows measuring the silt or clay concentration within the effluent which is expressed as the ratio of the mass of fine particles to water mass within the fluid with a maximum relative error of 5%. The time integration of the fine particle concentration gives the cumulative eroded dry mass for the corresponding duration (Bendahmane et al. 2008) with a maximum relative error of 7%.

The data acquisition is provided by a software which was written by the authors with LABVIEW (Laboratory Virtual Instrument Engineering Workbench). This code also draws automatically the time evolutions of hydraulic conductivity, hydraulic gradient, effluent mass, gradient of pressure and flow rate during entire test phases.

Test Materials and Test Procedure

SOIL GRADATIONS AND POTENTIAL SUSCEPTIBILITY TO SUFFUSION

Two non plastic soils were selected with a slight variation of grain size distributions to investigate suffusion susceptibility. A laser diffraction particle-size analyzer was used to measure the grain size distribution of the tested soils (see Fig. 6) with demineralized water and without a deflocculation agent. Both soils were created by mixing different materials. The gap-graded soil B is composed by the mixture of sand S1 (25%) and gravel G3 (75%) marketed by Sablière Palvadeau (France). The widely-graded soil R3 is created by the mixture of 28% sand S1 and 72% gravel from a French dike.

According to grain size based criterion proposed by Kenney and Lau (1985) both soils B and R3 are indeed internally unstable (see Table 1). For the soil B, P (the percentage finer than 0.063 mm) is less than 10% and the gap ratio $G_r = d_{max}/d_{min}$ (d_{max} and d_{min}: maximal and minimal particle sizes characterizing the gap in the grading curve) is smaller than 3, thus Chang and Zhang's (2013) method assessed the soil B as internally stable. For the soil R3, as the percentage of fine P is less than 5% and $(H/F)_{min} < 1$ (F, mass percentage of grains lower than d; H, mass percentage of grains between d and $4d$) Chang and Zhang's (2013) method classified this soil as internally unstable. According to Wan and Fell (2008), the method that they proposed seems not to be applicable for gap-graded soils and soils with a mass of fine fraction lower than 15%. Further this method is only relevant for soil R3 which is

classified as internally stable. Finally, even if these two gradations slightly differ, no clear classification can be drawn for soils B and R3 applying the three used criteria. Therefore, the erodibility characterization needs suffusion tests.

SPECIMEN PREPARATION

Eight multilayer specimens were prepared by moist compaction to prevent soil segregation and per layers of 5 cm in height (see Fig. 1) in order to limit the heterogeneity. Each layer was produced by using a static compaction technique to limit the soil anisotropy, until the fixed density and a specimen height of 350 mm were reached. All vertical and horizontal specimens were subjected to an axial stress of 200 kPa through the piston and the pore opening size of the downstream mesh is 1.2 mm in order to allow the erosion of all fine particles.

The saturation step began with the injection of carbon dioxide (from the bottom) for a duration of ten minutes to improve dissolution of gases into water and afterward, the specimen was saturated with tap water in upward direction by gradually increasing the level of the upstream tank (see Fig. 1). For preventing soil segregation in the specimen, to minimize the applied hydraulic gradient and to achieve a high degree of saturation, the free surface rose with a constant velocity of about 2 cm/h until it reached the top of the specimen. Approximately 24h were necessary for the water level to reach the specimen top. With horizontal #1 flow, all of the steps were identical to steps for vertical flow but after saturation, the specimen was turned from vertical to horizontal. The first beaker in the rotating sampling system was used to collect the particles lost during the saturation step. At the end of each test, the eroded fine particles caught by the linen bags were dried in an oven for 24 hours and their mass determined. The values of the initial dry density were determined by considering: (1) the soil mass

placed in the cell, (2) the loss mass during saturation phase and (3) the specimen height after saturation. The initial dry density of each specimen is shown in Table 2.

SUFFUSION TEST PROCEDURE

Specimens were subjected to a seepage flow under multistage hydraulic gradient, in downward direction or horizontal direction. For the purpose of improving readability, the name of each test starts by the soil letter. The second letter, V or H clarifies the vertical or horizontal flow direction. Table 2 details the characteristics of all performed tests.

During experiment, the upstream reservoir was fixed and the downstream reservoir was moved down step by step to stop at several predefined positions to apply the multi-stage hydraulic gradient. Fig. 7a and Fig. 7b show the multi-stage hydraulic gradient applied on specimens of soil, under vertical and horizontal directions, respectively. It can be noted that quite the same history of hydraulic gradient was applied under both flow directions. A beaker with linen bag in the rotating sampling system (see Fig. 5) is selected for the duration of each stage of hydraulic gradient. Finally, the repeatability of our specimen preparation and testing procedure was verified by performing two tests under identical conditions: B-V and B-V rep.

COMPUTATION OF HYDRAULIC CONDUCTIVITY AND EROSION RATE

The computation of hydraulic conductivity is based on the Darcy' formula.

$$k = \frac{Q}{i\,S} \tag{4}$$

where *i* is the hydraulic gradient and *S* is the cross-sectional area of flow.

The erosion rate is computed by:

$$\dot{m} = \frac{m_{eroded}\ (\Delta t)}{S\,\Delta t} \tag{5}$$

where $m_{eroded}(\Delta t)$ is the mass of eroded particles during the duration Δt.

In the case of vertical flow or horizontal flow along specimen length, the cross-sectional area of flow corresponds to the cross section of the specimen. Whereas in the case of horizontal flow along specimen diameter, the cross-sectional area of flow is expressed by:

$$S = \frac{S_{min}+S_{max}}{2} \quad (6)$$

where S_{min} is the flow section at the horizontal inlet and outlet with the 10 mm diameter of pipe and S_{max} is the biggest rectangular flow area: $S_{max} = D\ h_{flow\text{-}max}$, where D is the specimen diameter and $h_{flow\text{-}max}$ is the height of flow. For identifying the surface area of horizontal flow, simulations with Plaxis software were carried out. Suffusion of the soil is not described with Plaxis, consequently these simulations assume that the soil is undisturbed by drag forces all along the seepage flow. For the boundary conditions, the specimen is modelled as closed boundary around the specimen except the holes in horizontal direction. A Plaxis analysis is needed for each type of soil, but for this study, it is assumed that the values of hydraulic conductivity in vertical direction and in horizontal direction are equal to the average of the measured values of the initial hydraulic conductivity for soil B (i.e., $3\ 10^{-3}$ m.s^{-1}). The soil is assumed to be saturated with a dry unit weight equal to the initial dry unit weight of specimens of soil B (i.e., 17.36 kN.m^{-3}). The difference of water head is set to 0.05 m and these simulations permit to compute the height: $h_{flow\text{-}max}$ = 10.80 cm (Le 2017).

ESTIMATION OF THE SUFFUSION SUSCEPTIBILITY

Le et al. (2018) performed a statistical analysis to identify the main parameters and to focus on those that can easily be measured on existing structures. This study is built on suffusion tests all performed under vertical downward flow. By distinguishing gap-graded and widely graded soils, the authors proposed an estimation of the erosion resistance index based on the initial dry density, the grain shape

(with the measurement of the internal friction angle φ) and the water sensitivity (with the measurement of the blue methylene value *VBS*). Of course, the grain size distribution is also considered with the measurement of the gap ratio G_r, the percentage P, d_5, d_{60} and d_{90} (diameters of the 5%, 60%, 90% mass passing, respectively). Table 3 details the values of each physical parameter used for this estimation which leads to the value of I_α for specimens of soil B and for R3 specimens equal to 3.1 and 3.7, respectively. Thus the corresponding classification for both tested soils is moderately erodible. It is worth noting that as the discrepancy of grain size distributions and specimen densities is slight, soil B appears slightly less resistant than soil R3.

Test Results and Discussion

SPECIMENS COMPOSED BY ONE SOIL

Two tests were carried out on soil R3, one under vertical flow (test R3-V) and the second under horizontal flow (test R3-H). Two specimens of soil B were performed under vertical flow (tests B-V and B-V rep) and two others under horizontal flow: along specimen length for test B-H#1 and along specimen diameter for B-H #2. The time evolution of hydraulic conductivity and erosion rate are shown in Fig. 8a and Fig. 8b for tests of soil R3 and in Fig. 9a and Fig. 9b for B tests.

Fig. 8a shows that the hydraulic conductivity of soil R3 under horizontal flow is higher than under vertical flow. Under both flow directions, the hydraulic conductivity is smaller than 1.5 10^{-3} m.s^{-1} and continuously decreases during the suffusion process. The erosion rate fluctuates during the testing process but it is always smaller than 9 10^{-4} kg.s^{-1}.m^{-2} (see Fig. 8b). The conjunction of hydraulic conductivity decreasing and small magnitude of erosion rate suggests that the predominant process induced by the seepage flow is the filtration process.

Fig 9a and Fig 9b first show that repeatability of specimen preparation is fairly good, as the initial values of hydraulic conductivity and erosion rate are very close for tests B-V and B-V rep. However, the time evolutions of both parameters are rather scattered. It is worth noting that the imprecision regarding the hydraulic conductivity computation is estimated at $\pm 0.8\ 10^{-4}$ m.s^{-1} for a flow along specimen height and at $\pm 1.0\ 10^{-4}$ m.s^{-1} for a flow along specimen diameter. The accuracy of the erosion rate measurement is estimated at $\pm 5\ 10^{-6}$ kg.s^{-1}.m^{-2}. Thus those spread-out results cannot be attributed to imprecision, but rather to the complexity of the suffusion process. For all tests on soil B, the initial hydraulic conductivity is between $2.4\ 10^{-3}$ m.s^{-1} and $4.6\ 10^{-3}$ m.s^{-1} and the erosion rate corresponding to the first hydraulic gradient stage is between $2.2\ 10^{-5}$ kg.s^{-1}.m^{-2} and $6.5\ 10^{-5}$ kg.s^{-1}.m^{-2}. It is worth stressing that under vertical flow, the hydraulic conductivity stays relatively constant during a stage of hydraulic gradient. However, when the erosion rate exceeds $5\ 10^{-4}$kg.s^{-1}.m^{-2}, the hydraulic conductivity starts to increase during a hydraulic gradient stage. Whereas, under horizontal flow, even with an erosion rate smaller than $5\ 10^{-4}$kg.s^{-1}.m^{-2}, the hydraulic conductivity can be higher than $5\ 10^{-3}$m.s^{-1}. Only test B-H#2 was performed under a parallel flow to the interface between soil layers, and for this test the hydraulic conductivity appears slightly higher. This result is in agreement with results of Pachideh and Mir Mohammad Hosseini (2019). At the end of all tests on soil B, the hydraulic conductivity is around $6\ 10^{-3}$m.s^{-1}.

With the objective to explain the discrepancy of the evolution of hydraulic conductivity of B specimens under vertical and horizontal flows, the post suffusion gradation was determined. The specimen B-V was divided into three parts: top, middle and bottom layers. With the same goal, specimen B-H#1 was frozen after suffusion test, in order to permit a longitudinal cut in top and bottom layers. These designations: top, middle and bottom of layer position are related to the vertical position and are not

338 relative to the flow direction. Moreover for specimen B-H#1, each layer was subdivided in upstream
339 and downstream parts (see Fig. 10). Fig. 11 a shows that under vertical flow, the largest decrease of
340 fine fraction is measured in the top layer (which corresponds to the upstream part of the specimen B-
341 V), followed by the middle layer. The post-suffusion fine fraction in top, middle and bottom layers is
342 about 19.2%, 21.5%, and 22.2%, respectively. These results are in agreement with the results of Ke and
343 Takahashi (2012) and they suggest that the transport of detached particles from upstream to
344 downstream parts can partly offset the loss of particles in the middle and downstream parts.
345 Under horizontal flow, Fig. 11b shows that for both layers, it is not possible to distinguish the gradation
346 of upstream and downstream parts. However, the percentage of fine particles is 17.4% in top layer and
347 it exceeds the initial percentage of fine in bottom layer, with around 27.4%. This result suggests that in
348 comparison with the loss of fine particles under vertical flow, the loss under horizontal flow is larger in
349 top layer, but the process of filtration is enhanced in bottom layer. Thus when the direction of flow is
350 perpendicular to gravity, the specimen becomes more heterogeneous and a preferential flow can
351 appear in the top layer. This explains why under this flow direction, the hydraulic conductivity is higher
352 and quite constant during the suffusion process.
353 Post-suffusion gradation of specimens R3-V and R3-H, are plotted in Fig. 12a and 12b respectively. The
354 results show a small loss of fine particles under horizontal flow but quite no variation of grain size
355 distribution under vertical flow. This result confirms that soil R3 is more resistant when undergoing
356 suffusion process. Thus the absence of gap in the gradation improves the auto-filtration.
357 Thanks to the measurement of the time variations of hydraulic gradient, flow rate and erosion rate, it
358 is possible to characterize the suffusion initiation by the mean of a critical value of: the hydraulic
359 gradient, the flow velocity or the hydraulic shear stress. However, the suffusion initiation is influenced

360 by the hydraulic loading path (Rochim et al. 2017). Moreover Zhong et al. (2018) showed that the critical
361 hydraulic gradient decreases with the flow length. Thereby the authors interpret the test results by the
362 energy based method and the cumulative loss of dry mass versus the cumulative expended energy of
363 soil B is shown in Fig. 13. As the applied hydraulic gradient was quite identical for all performed tests,
364 Figure 13 shows for all tests on soil B , the same trend of suffusion development. For a final cumulative
365 expended energy comprised between 500 and 1000 J, the cumulative loss dry mass is between 0.05
366 and 0.2 kg. At the steady state, which corresponds to the final data point for all tests, the erosion
367 resistance index (I_α) is computed by equation (3). Under vertical flow the value of I_α for test B-V and B-
368 V rep is 3.8 and 3.7, respectively. The corresponding suffusion classification is moderately erodible.
369 Under horizontal flow, the classification is moderately resistant corresponding to the erosion resistance
370 index equal to 4.0 for test B-H#2 and 4.1 for test B-H#1. It is worth noting that these values are close,
371 highlighting the ability to characterize with accuracy, the suffusion susceptibility under horizontal flow
372 in both conditions, i.e., #1 and #2. The comparison of the results of these four tests shows that the soil
373 B appears slightly more resistant under horizontal flow. Similarly, Fig. 14 shows the cumulative loss dry
374 mass versus expended energy of soil R3. As this soil is slightly less permeable than soil B, under quite
375 identical multi-stage hydraulic gradient, the final cumulative expended energy is slightly smaller and
376 comprised between 300 and 800 J. However, the cumulative loss dry mass is also slightly smaller and
377 between 0.01 and 0.03 kg. At steady state, the erosion resistant index is equal to 4.3 and 4.4 under
378 vertical and horizontal flows, respectively. These results confirm that in comparison with soil B, the soil
379 R3 is more resistant (i.e., classified as moderately resistant) and both tested soils appear less resistant
380 to suffusion process under vertical flow.

It should be noted that in literature, most of the tests were performed under vertical flow and this study shows that in this case, the value of the erosion resistance index could be slightly underestimated. Consequently, the authors consider that a modification of the suffusion chart proposed by Marot et al. (2016) appears not necessary, because it only induces a slight conservatism for horizontal flow.

SPECIMENS COMPOSED BY TWO SOILS

A real earth structure is generally built by the compaction of several soil layers which are globally horizontal, whereas the core sample is generally realized in vertical. In consequence a sample obtained by core sampling in site may be composed by several layers of soils, which slightly differ by their gradations with a horizontal interface. As already mentioned, the most often used method for suffusion tests consists to apply a vertical flow (i.e., perpendicular with the interface). In this context, a specimen B/R3-V was prepared by moist compaction of 4 layers of soil B topped with 3 layers of soil R3. Then, it was subjected to a vertical flow and the evolution of the cumulative loss mass depending on the cumulative expended energy is slightly the same as for specimen R3-V (see Fig. 14). At the steady state, the value of I_α is equal to 4.6 and consequently, the suffusion classification is moderately resistant, as soil R3.

By contrast, in site the flow is generally horizontal and parallel with the interface of soil layers. The specimen B/R3-H (prepared under identical condition as specimen B/R3-V) was subjected to a horizontal flow in condition #2, which means a flow parallel with the interface between the two soils. Fig. 14 shows that the cumulative loss mass versus the cumulative expended energy is very close to the result of test B-H#2 and with the same I_α value of soil B (i.e., 4.0).

Conclusions

A new device and associated data acquisition code were developed in order to give the opportunity to perform suffusion tests on undisturbed specimen and to allow applying a vertical or a horizontal flow. Two cohesionless soils which slightly differ by their grain size distributions were selected. Eight specimens were prepared by moist and static compaction to limit the soil anisotropy. The energy based method is used to compute the erosion resistance index at the steady state (i.e., when the hydraulic conductivity tends to stabilize and the erosion rate tends to decrease). By this way, the suffusion susceptibility is classified.

First, a series of suffusion tests was carried out under vertical or horizontal flow on specimens composed by one soil. The test results show that the repeatability of specimen preparation is fairly good. Under horizontal flow, both tested soils appear more permeable, and they are also slightly more resistant to suffusion process. The comparison of post-suffusion gradations with the initial ones permits to note that under horizontal flow, the specimens become more heterogeneous with a higher loss of fine particles in the top layer. A preferential flow can then appear in this layer which limits the suffusion development and explains the higher hydraulic conductivity. Thus, these results demonstrate the significant influence of the seepage flow direction on the suffusion susceptibility.

Two specimens were composed of a layer of each tested soils. When the injected flow is perpendicular to the interface between soil layers, the suffusion susceptibility is mainly influenced by the more resistant soil. By contrast, the suffusion susceptibility is mostly influenced by the less resistant soil in the case of a parallel flow to the interface.

Therefore in the comparison with the mostly used configuration of suffusion test (i.e., flow perpendicular to the interface between soil layers), the new device permits to avoid a slight overestimation of the soil strength face to suffusion susceptibility.

This new device and the energy based method permit to assess the suffusion soil susceptibility, which is a material property. Thanks to this energy based method and tests performed with this device under various hydraulic loading paths, a relation will be proposed between the hydraulic loading and the corresponding soil response in time.

ACKNOWLEDGMENTS

The authors thank the company IMSRN, the Ministry of Education and Training of Vietnam, the University of Danang, Vietnam, for providing financial support for this work.

References

Bendahmane, F., D. Marot, and A. Alexis. 2008. “Experimental parametric study of suffusion and backward erosion,” *J. Geotech. Geoenviron. Eng.*, Vol. 134, No .1, pp. 57-67.

Briaud, J. L. 2008. “Case Histories in Soil and Rock Erosion: Woodrow Wilson Bridge, Brazos River Meander, Normandy Cliffs, and New Orleans Levees,” *J. Geotech. Geoenviron. Eng.*, Vol. 134, No. 10, pp. 1425-1447.

Chang, D. S., and L. M. Zhang. 2011. “A stress-controlled erosion apparatus for studying internal erosion in soils,” *Geotech. Test. J.,* Vol. 34, No. 6, pp. 579-589.

Chang, D.S., and L.M. Zhang. 2013. “Extended internal stability criteria for soils under seepage,” *Soils Found.,* Vol. 53, No. 4, pp. 569-583.

441 Fell, R., and J. J. Fry. 2013. "Erosion in geomechanics applied to dams and levees," Bonelli S. Editor.,
442 *ISTE-Wiley.*, pp. 1-99.
443 Foster, M., R. Fell, and M. Spanagle. 2000. "The statistics of embankment dam failures and accidents,"
444 *Can. Geotech. J.,* Vol. 37, No. 5, pp. 1000-1024.
445 Fry, J. J., A. Vogel, P. Royet, and J. R. Courivaud. 2012. "Dam failures by erosion: Lessons from ERINOH
446 data bases," Proc., *6th Int. Conf. on Scour and Erosion*, Paris, pp. 273-280.
447 Hanson, G. J., and A. Simon. 2001. "Erodibility of cohesive streambeds in the loess area of the
448 Midwestern, USA," *Hydrological Processes*, Vol. 15, No. 1, pp. 23–38
449 Ke, L., and A. Takahashi. 2012. "Strength reduction of cohesionless soil due to internal erosion induced
450 by one-dimensional upward seepage flow," *Soils Found.,* Vol. 52, No. 4, pp. 698-711.
451 Ke, L., and A. Takahashi. 2014. "Experimental investigations on suffusion characteristics and its
452 mechanical consequences on saturated cohesionless soil," *Soils Found.,* Vol. 54, No. 4, pp. 713-730.
453 Kenney, T. C., and D. Lau. 1985. "Internal stability of granular filters," *Can. Geotech. J.,* Vol. 22, No. 2,
454 pp. 215-225.
455 Le, V.T. 2017. "Development of a new device and statistical analysis for characterizing soil sensibility
456 face suffusion process," PhD Thesis, University of Nantes, France, 202p.
457 Le, V.T., D. Marot, A. Rochim, F. Bendahmane, and H. H. Nguyen. 2018. "Suffusion susceptibility
458 investigation by energy based method and statistical analysis," *Can. Geotech. J.,* Vol. 55, No. 1, pp
459 57-68,
460 Marot, D., F. Bendahmane, F. Rosquoet, and A. Alexis. 2009. "Internal flow effects on isotropic confined
461 sand-clay mixtures," *Soil & Sediment Contamination*, Vol. 18, No. 3, pp. 294-306.

462 Marot, D., P. L. Regazzoni, and T. Wahl. 2011a. "Energy based method for providing soil surface
463 erodibility rankings," *J. Geotech. Geoenviron. Eng.*, Vol. 137, No. 12, pp. 1290-1293.
464 Marot, D., F. Bendahmane, and J. M. Konrad. 2011b. "Multichannel optical sensor to quantify particle
465 stability under seepage flow," *Can. Geotech. J.,* Vol. 48, No. 12, pp. 1772-1787.
466 Marot, D., F. Bendahmane, and H. H. Nguyen. 2012. "Influence of angularity of coarse fraction grains
467 on internal erosion process," *La Houille Blanche,* No. 6, pp. 47-53.
468 Marot, D., A. Rochim, H. H. Nguyen, F. Bendahmane, and L. Sibille. 2016. "Assessing the susceptibility
469 of gap graded soils to internal erosion characterization: proposition of a new experimental
470 methodology," *Nat. Hazards*, Vol. 83, No. 1, pp. 365-388.
471 Moffat, R., and R. J. Fannin. 2006. "A large permeameter for study of internal stability in cohesionless
472 soils," *Geotech. Test. J.,* Vol. 23, No. 1, pp. 116-122.
473 Moffat, R., R. J. Fannin, and S. J. Garner. 2011. "Spatial and temporal progression of internal erosion in
474 cohesionless soil," *Can. Geotech. J.,* Vol. 48, No. 3, pp. 399-412.
475 Pachideh, V., and S. M. Mir Mohammad Hosseini. 2019. "A new physical model for studying flow
476 direction and other influencing parameters on the internal erosion of soils", *Geotech. Test. J.,*
477 https://doi.org/10.1520/GTJ20170301.ISSN 0149-6115.
478 Patent. 2018. "System and process of soil erosion measurement", *European Patent Office* 28/11/2018,
479 No. 18209007.6. – 1001.
480 Rochim, A., D. Marot, L. Sibille, and V. T. Le. 2017. "Effect of hydraulic loading history on suffusion
481 susceptibility of cohesionless soils," *J. Geotech. Geoenviron. Eng.*, Vol. 143, No. 7, DOI
482 10.1061/(ASCE)GT.1943-5606.0001673.

Sail, Y., D. Marot, L. Sibille, and A. Alexis. 2011. "Suffusion tests on cohesionless granular matter," *Eur. J. Environ. Civ. Eng.*, Vol 15, No. 5, pp. 799-817.

Sibille, L., F. Lominé, P. Poullain, Y. Sail, and D. Marot. 2015. "Internal erosion in granular media: direct numerical simulations and energy interpretation," *Hydrological Processes*, Vol 29, No. 9, pp. 2149-2163.

Skempton, A. W., and J. M. Brogan. 1994. "Experiments on piping in sandy gravels," *Géotechnique*, Vol. 44, No. 3, pp. 440-460.

Slangen, P., and R. J. Fannin. 2017. "A flexible wall permeameter for investigating suffusion and suffosion," *Geotech. Test. J.,* Vol. 40, No. 1, pp. 1-14.

Smith, M., and J. M. Konrad. 2011. "Assessing hydraulic conductivities of a compacted dam core using geostatistical analysis of construction control data," *Can. Geotech. J.* Vol. 48, No. 9, pp. 1314-1327.

Wan, C. F., and R. Fell. 2004. "Investigation of rate of erosion of soils in embankment dams", *J. Geotech. Geoenviron. Eng., Vol.*130, No. 4, pp. 373–380

Wan, C. F., and R. Fell. 2008. "Assessing the potential of internal instability and suffusion in embankment dams and their foundations," *J. Geotech. Geoenviron. Eng.*, Vol. 134, No. 3, pp. 401-407.

Zhong, C., V. T. Le, F. Bendahmane, D. Marot, and Z. Y. Yin. 2018. "Investigation of spatial scale effects on suffusion susceptibility," *J. Geotech. Geoenviron. Eng.*, Vol. 144, No. 9, DOI: 10.1061/(ASCE)GT.1943-5606.0001935.

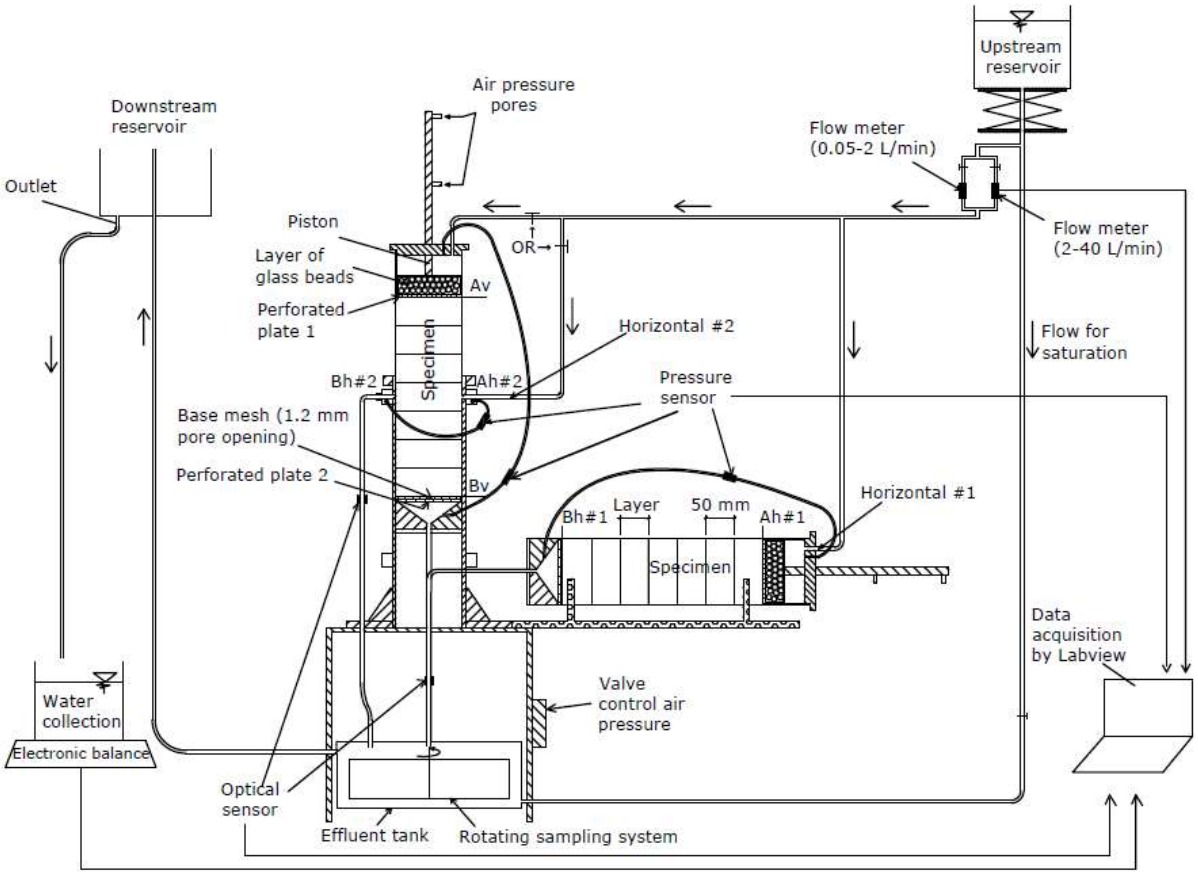

503

504 **FIG. 1** Overview of the multidirectional flow apparatus. The positions of upstream and downstream sections

505 are shown for vertical flow by: Av and Bv; and for horizontal flow by: Ah#1 and Bh#1 or Ah#2 and Bh#2 under

506 condition #1 or #2, respectively.

507

508

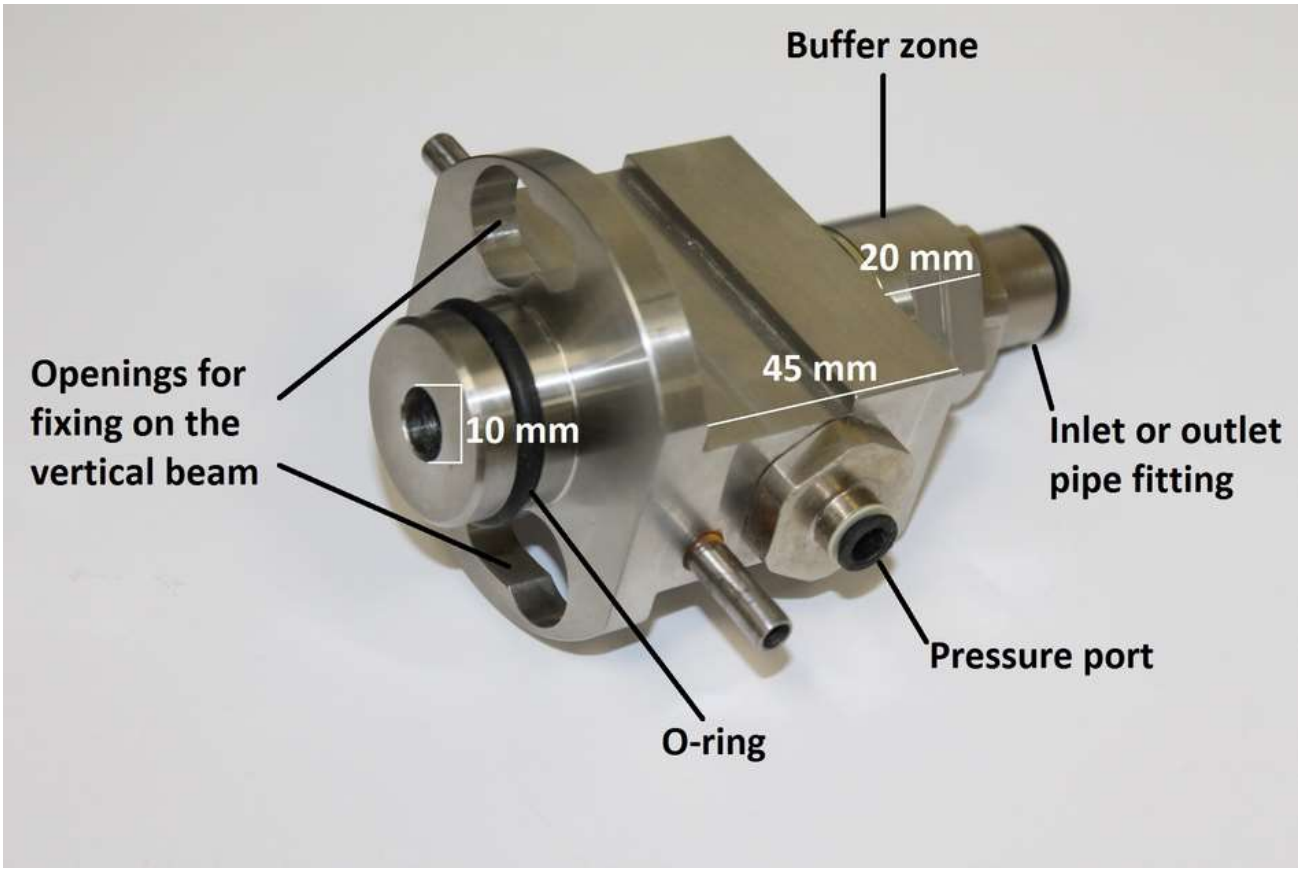

509

510 **FIG. 2** Components of inlet #2 and outlet #2.

511

512

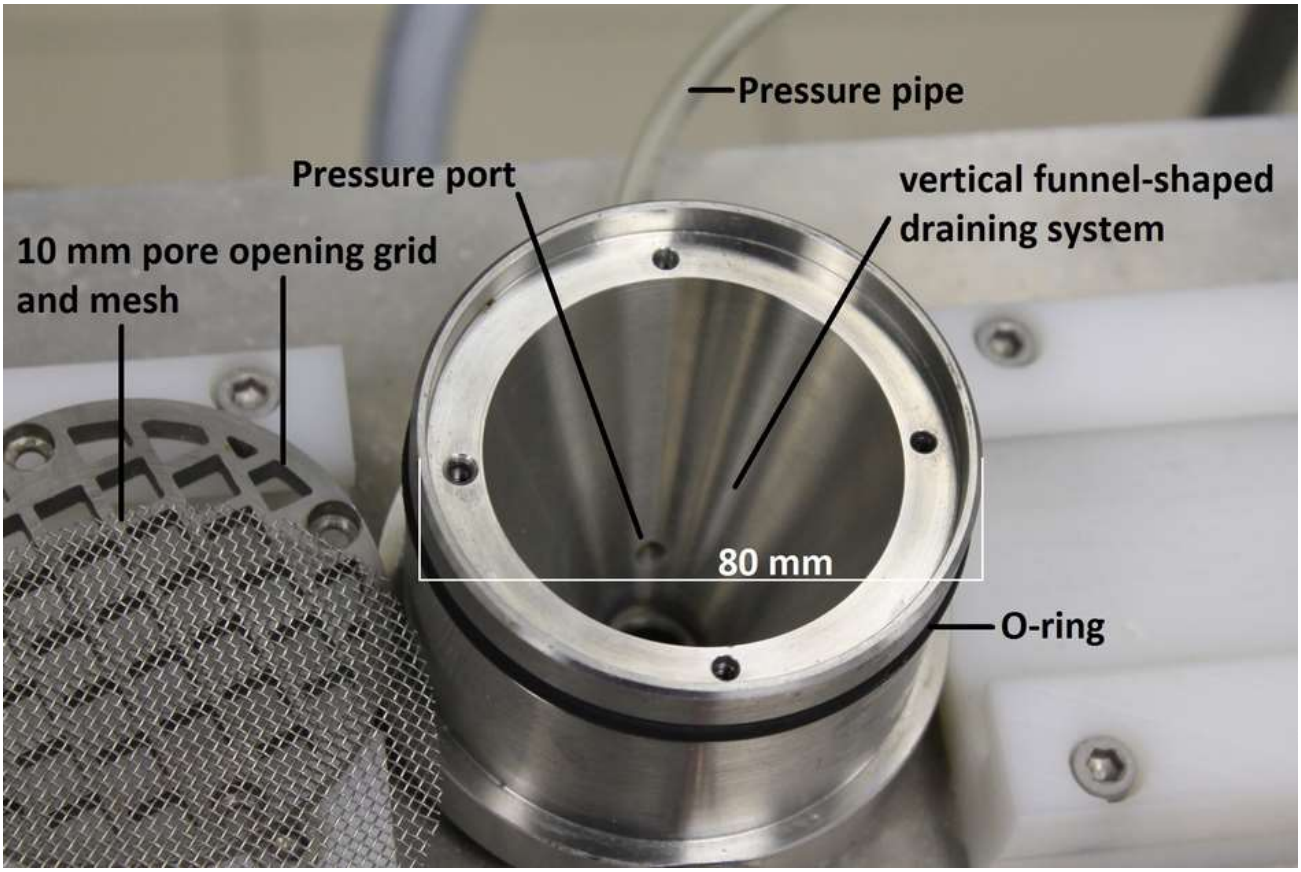

FIG. 3 Base pedestal with 10 mm pore opening grid and mesh, O-ring and pressure port.

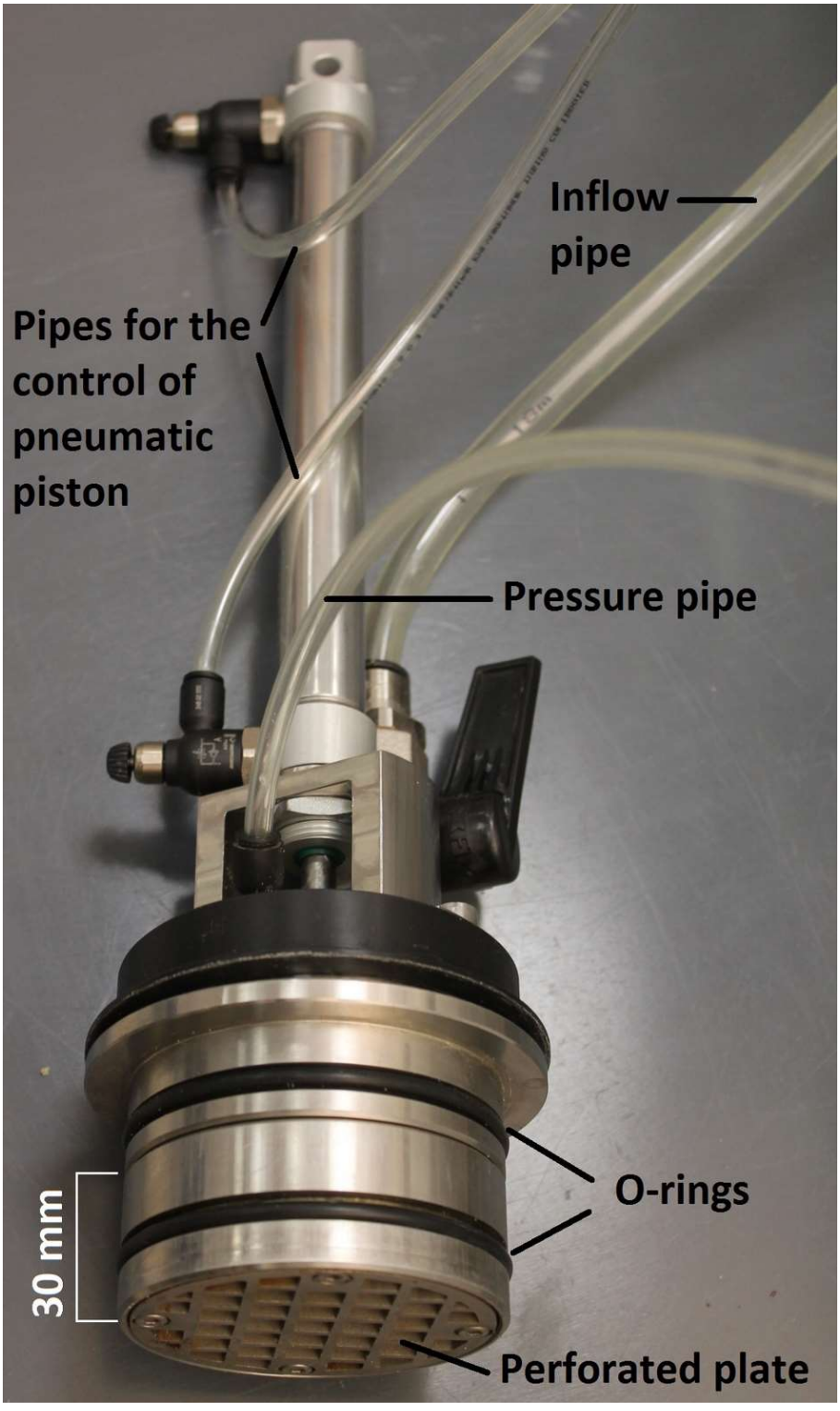

FIG. 4 Piston with 10 mm pore opening grid, O-ring, pipes for the control of pneumatic piston and pressure port.

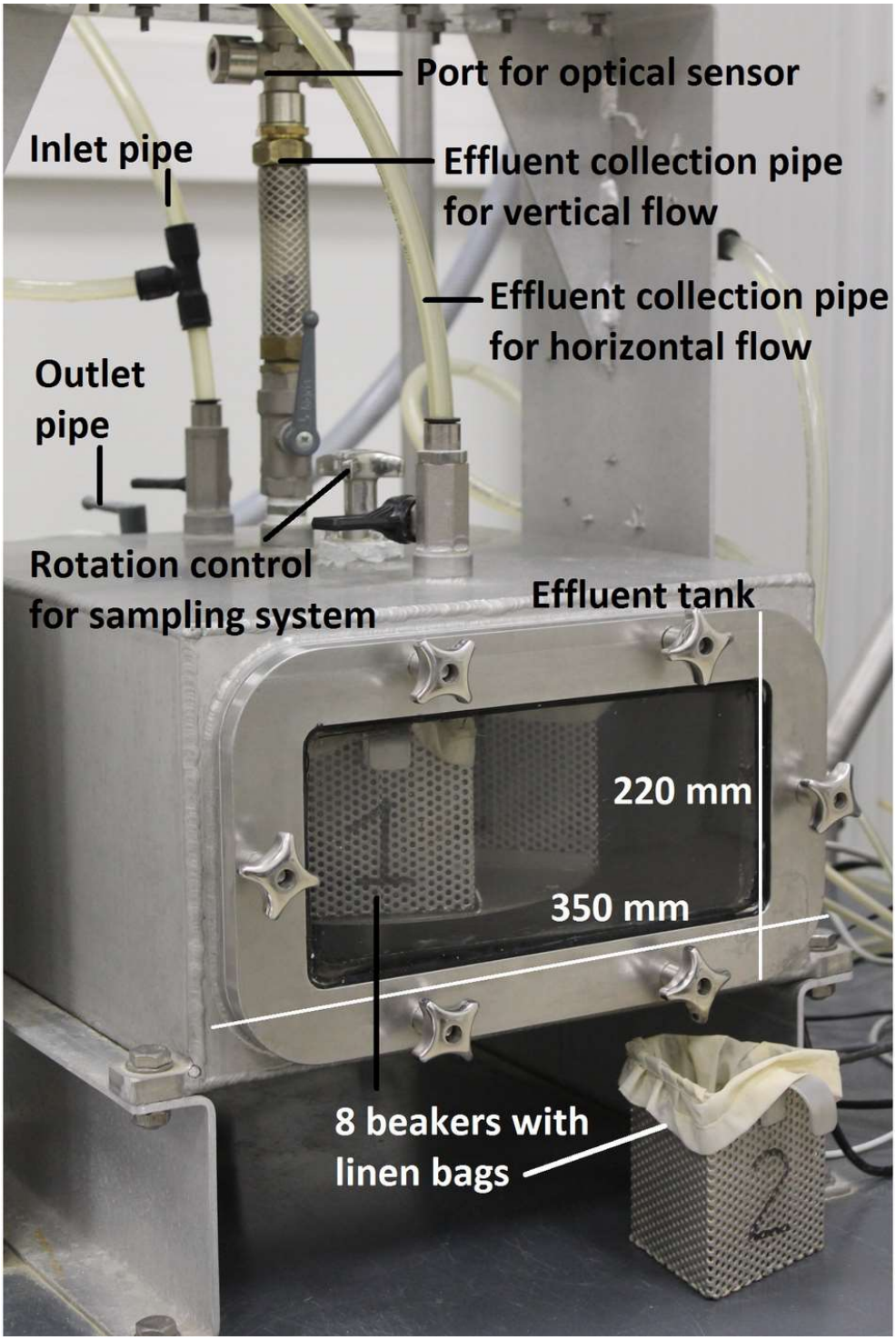

520

521 **FIG. 5** Soil collection system.

522

523

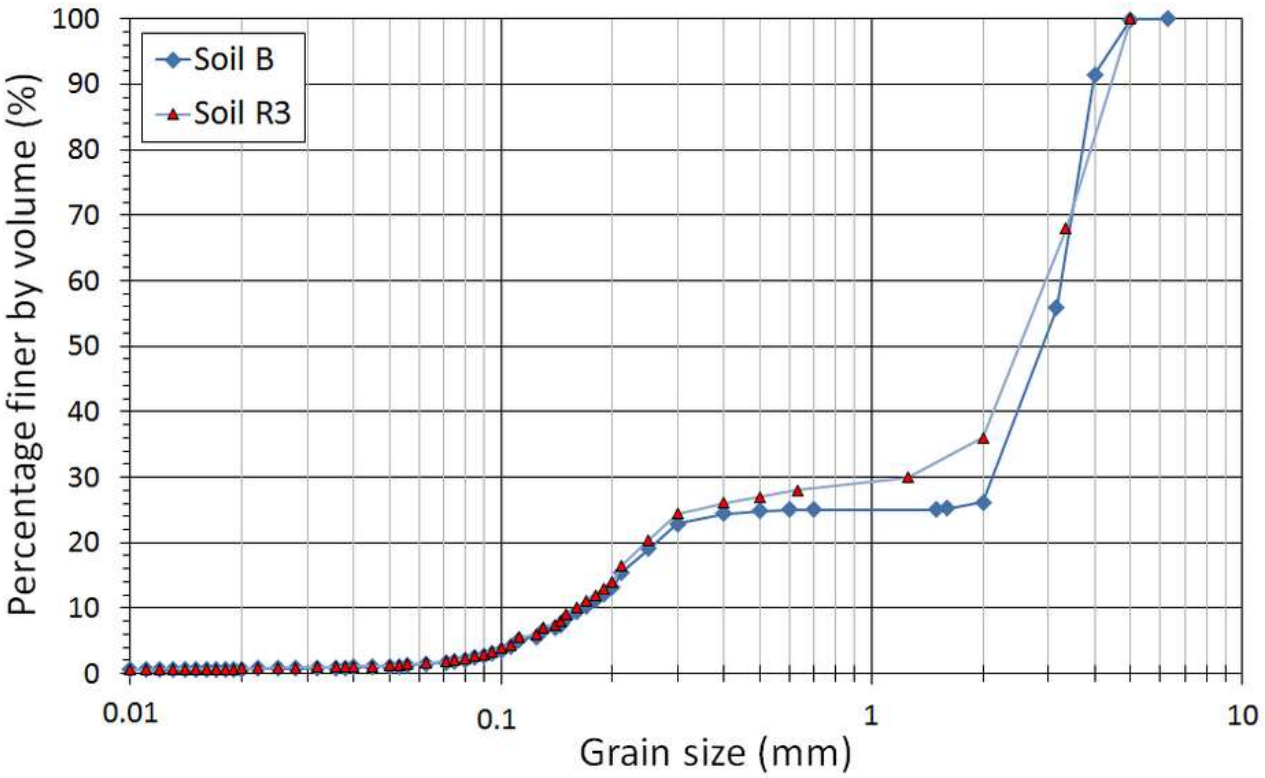

524

525 **FIG. 6** Grain size distribution of tested soils.

526

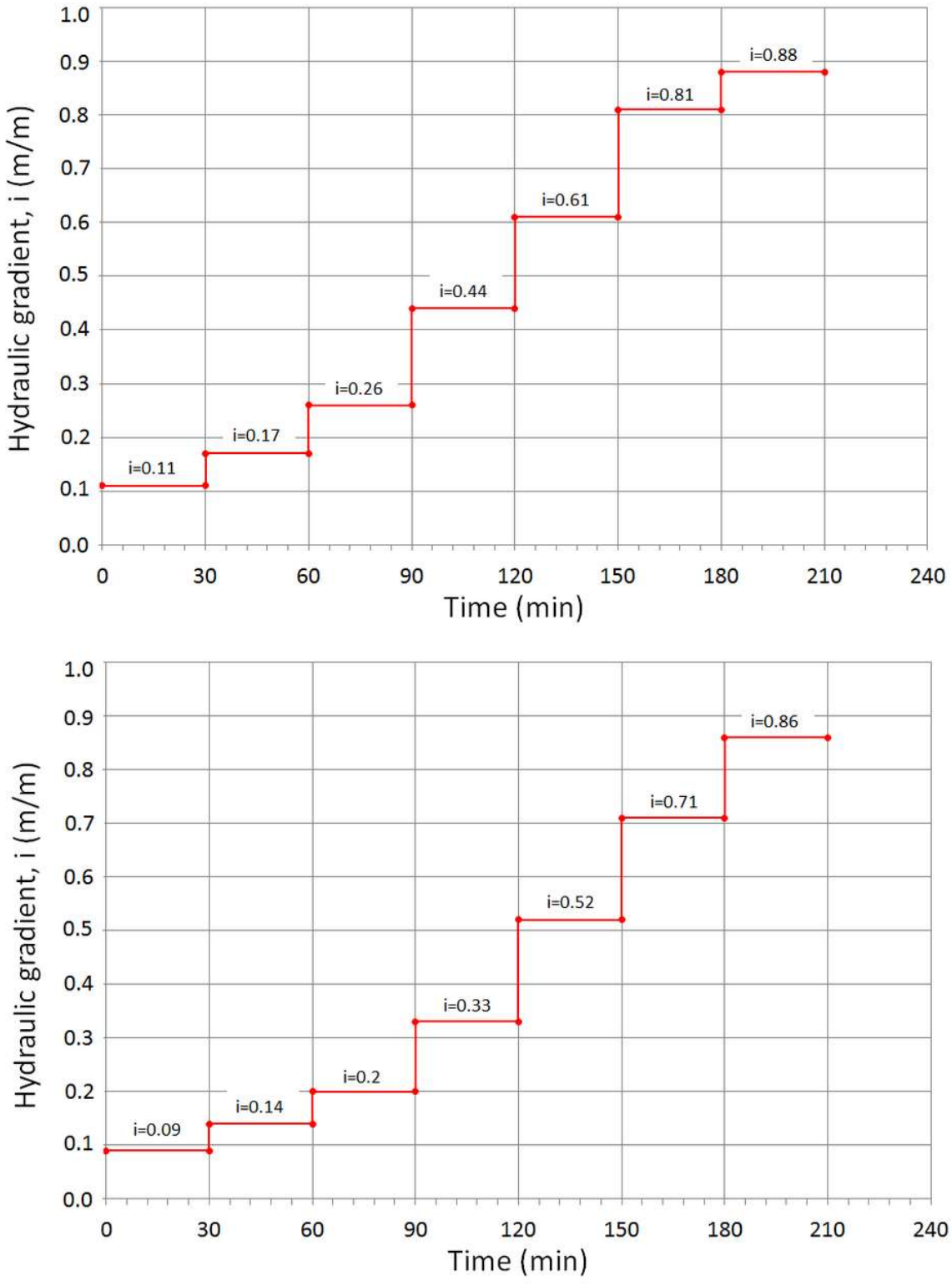

527

528 **FIG. 7** Multi-stage hydraulic gradient for test (a) under vertical flow and (b) under horizontal flow.

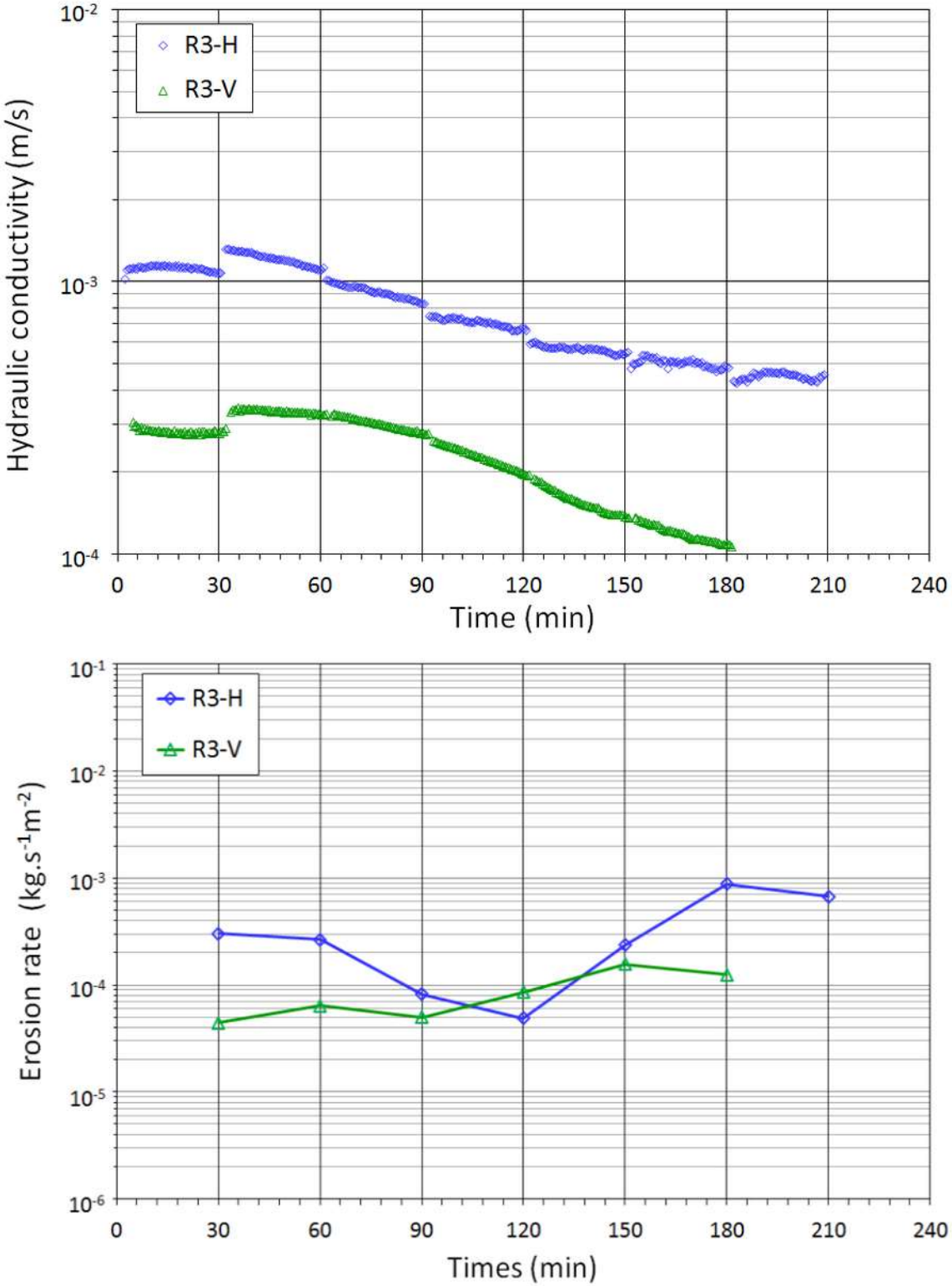

FIG. 8 Time evolution of (a) hydraulic conductivity of soil R3 and (b) erosion rate of soil R3.

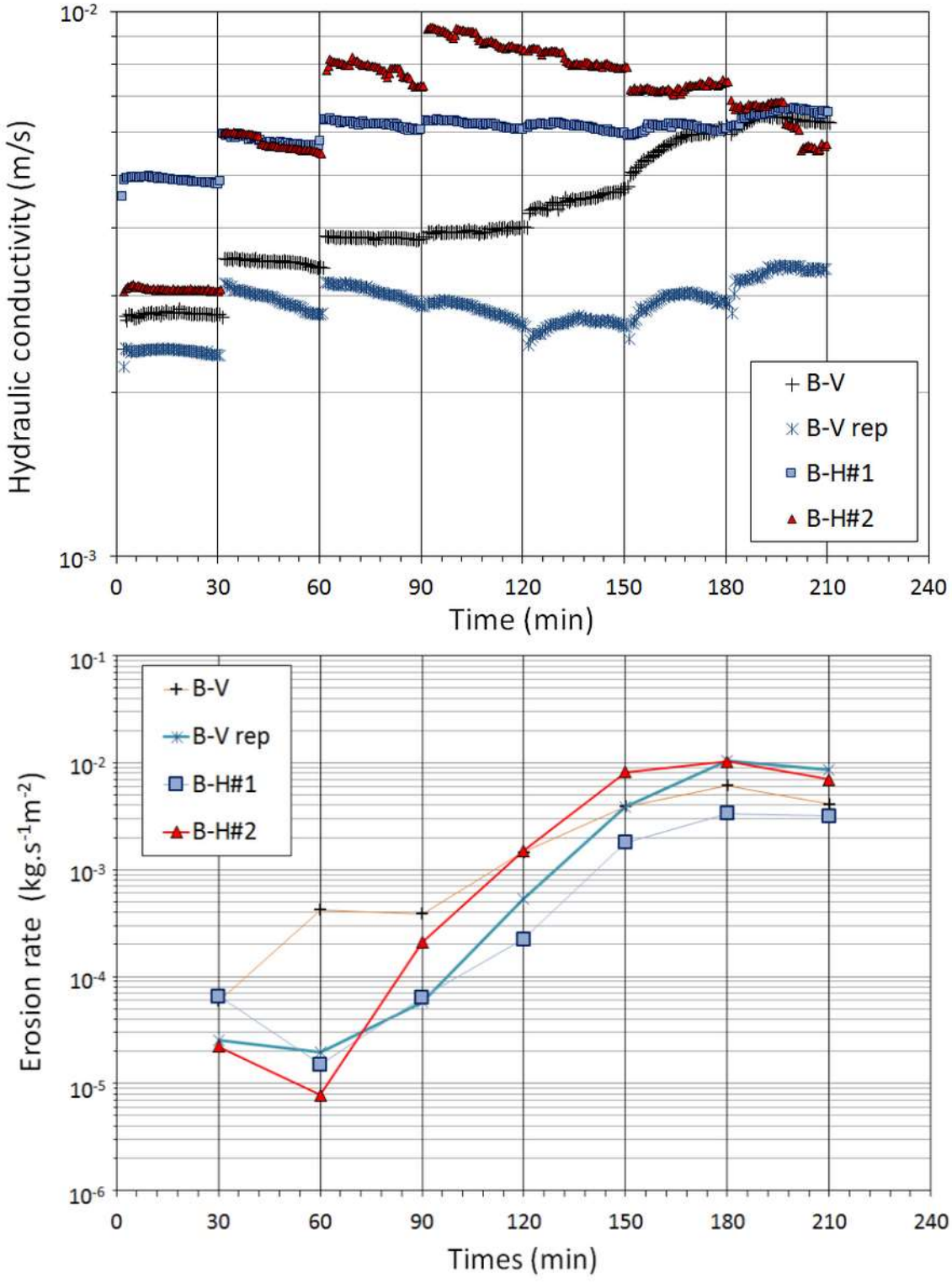

531

532 **FIG. 9** Time evolution of (a) hydraulic conductivity of soil B and (b) erosion rate of soil B.

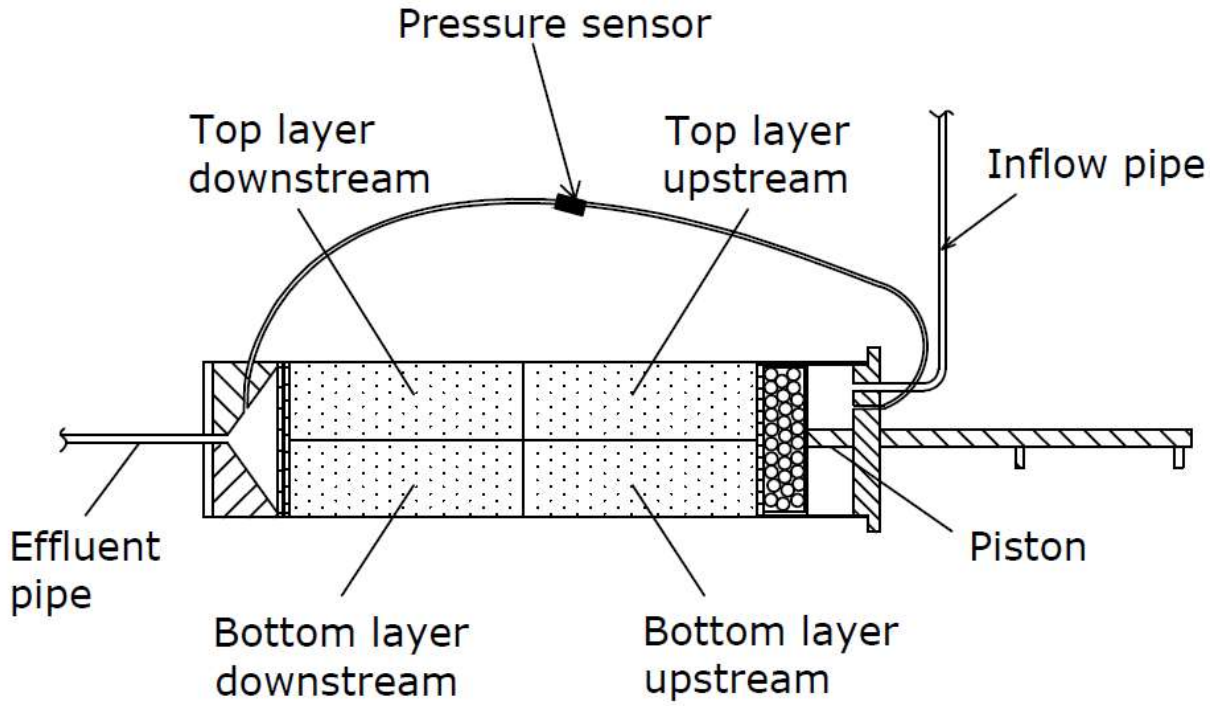

533

534 **FIG. 10** Position of layers for post-suffusion gradation of specimen B-H#1

535

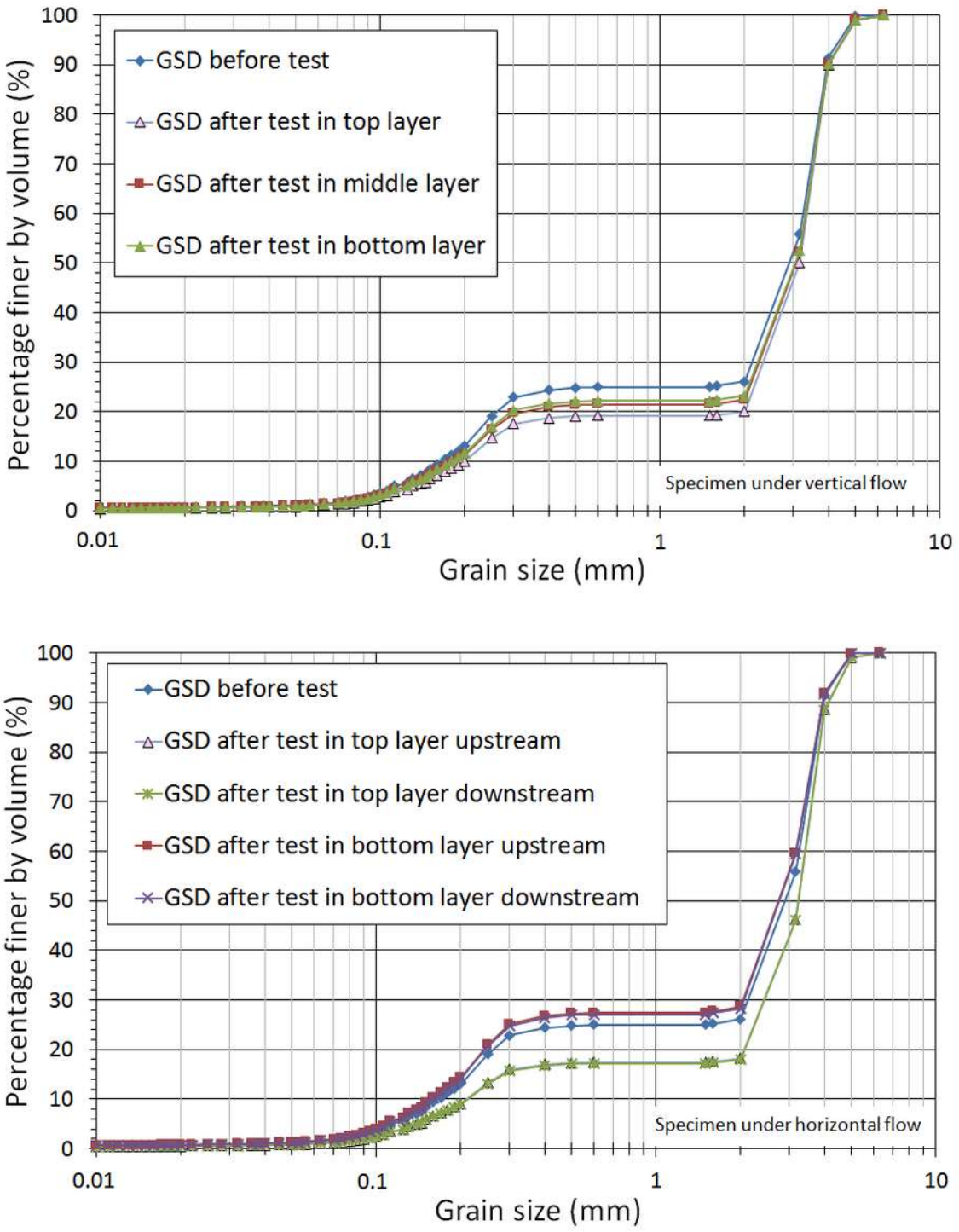

536

537 **FIG. 11** Grain size distribution of soil B (a) under vertical flow and (b) under horizontal flow.

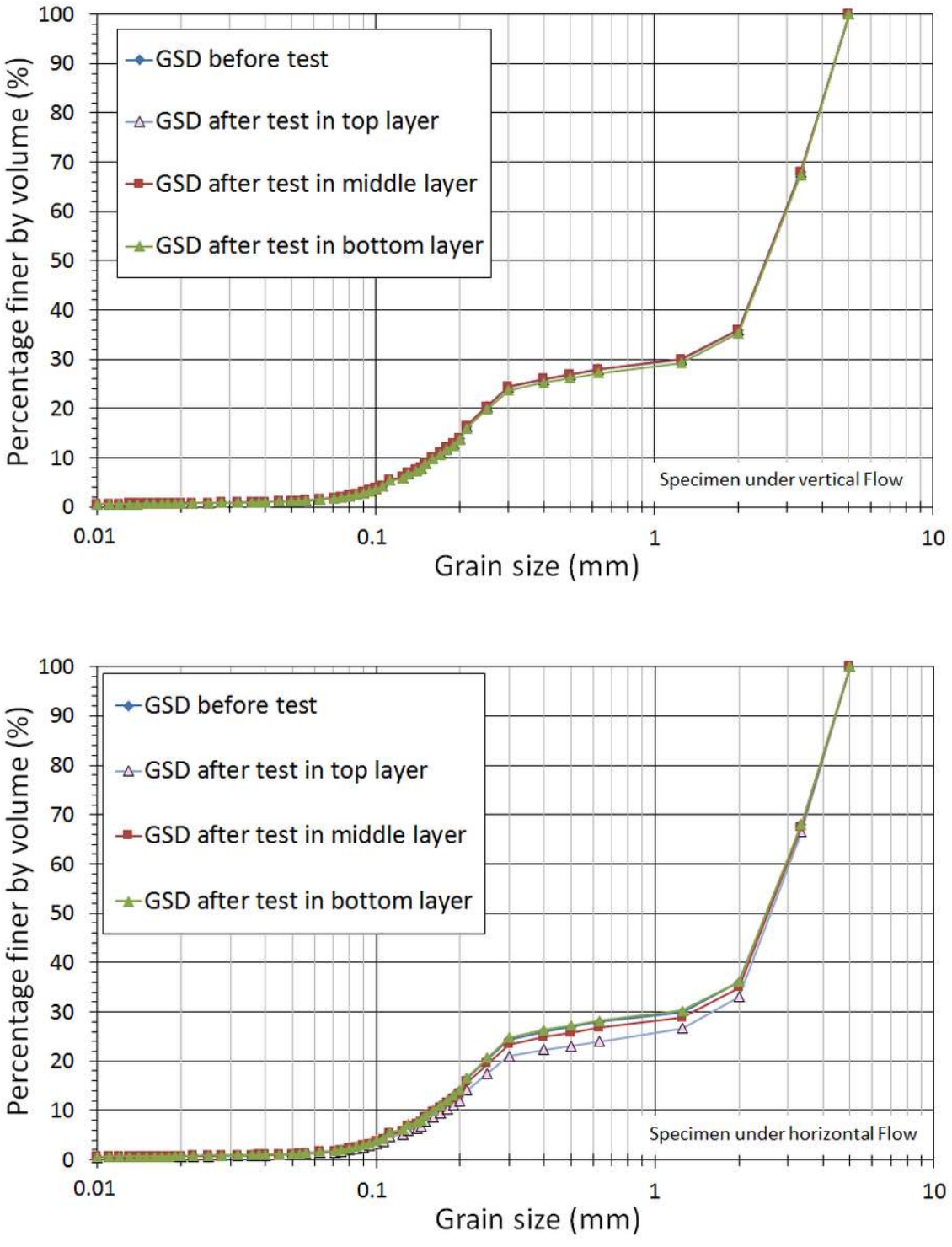

538

539 **FIG. 12** Grain size distribution of soil R3 (a) under vertical flow and (b) under horizontal flow.

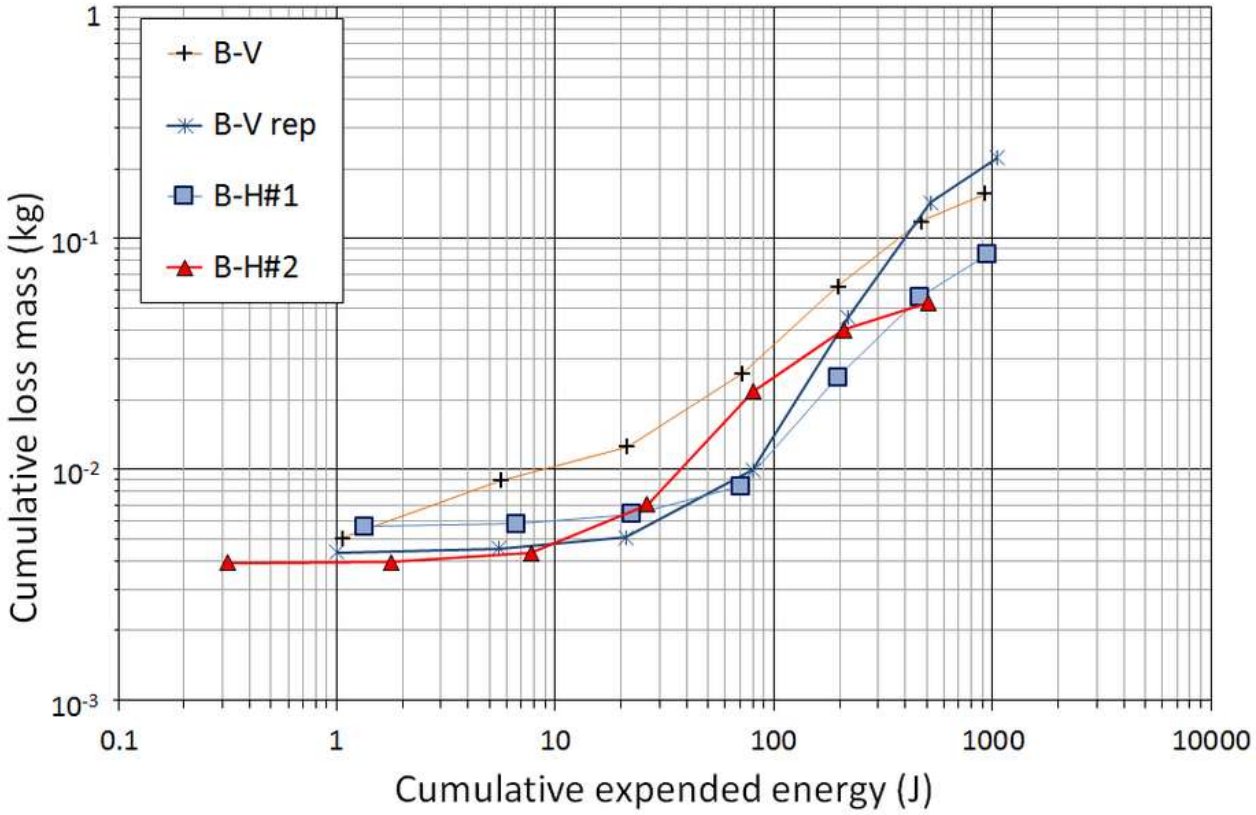

540

541 **FIG. 13** Cumulative loss mass versus cumulative expended energy under both flow directions of soil B.

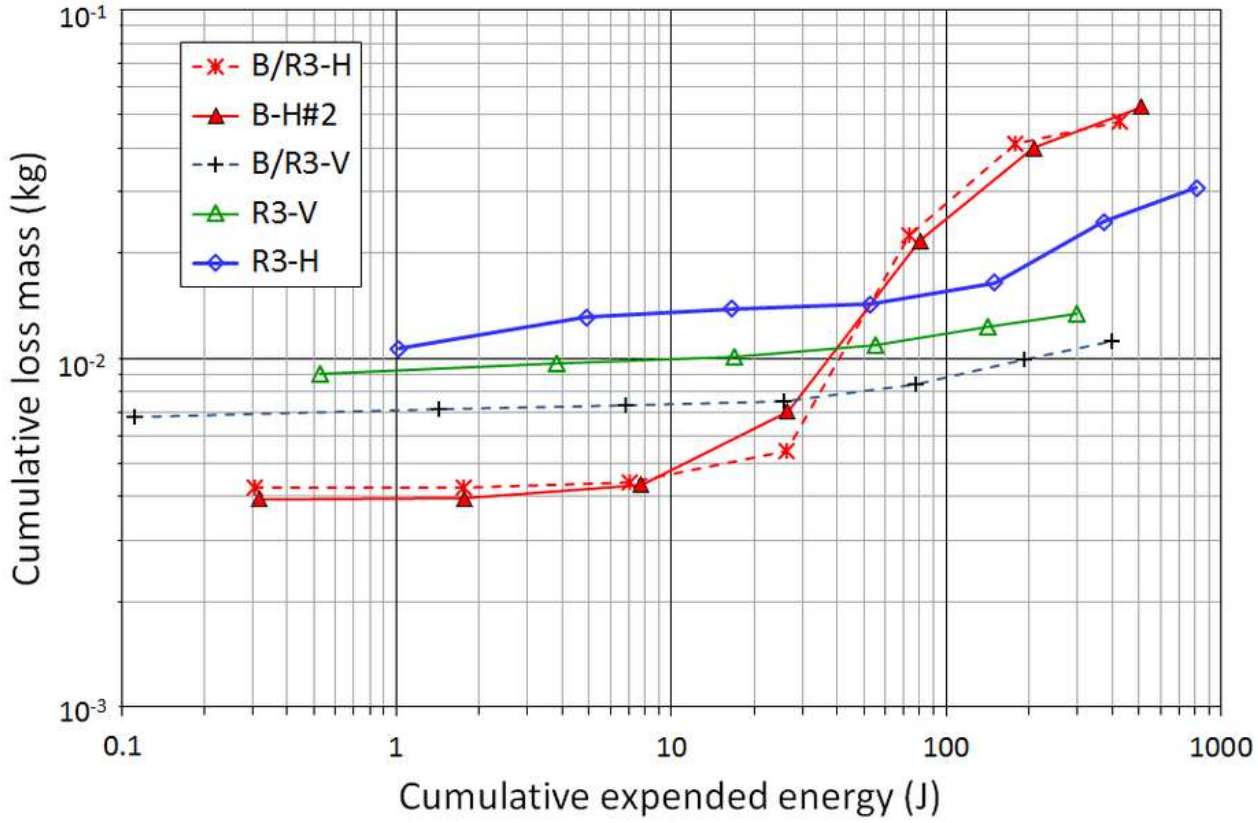

542

543 **FIG. 14** Cumulative loss mass versus cumulative expended energy under both flow directions of specimens R3

544 and B/R3.

545

Table 1 Characteristics of tested gradations and potential of suffusion susceptibility.

Tested gradation	P (%)	G_r	C_u	d_{15}/d_{85}	$(H/F)_{min}$	D $(H/F)_{min}$ (mm)	Kenney and Lau's criterion	Wan and Fell's criterion	Chang and Zhang's criterion
B	1.6	2.5	19.52	0.054	0.035	0.400	U	/	S
R3	1.2	1	16.23	0.046	0.208	0.335	U	S	U

Note: P = percentage of particle smaller than 0.063mm; $G_r = d_{max}/d_{min}$ (d_{max} and d_{min}: maximal and minimal particle sizes characterizing the gap in the grading curve); C_u = uniformity coefficient; d_{15} and d_{85} are the sieve sizes for which 15% and 85% respectively of the weighed soil is finer; F and H are the mass percentages of the grains with a size, lower than a given particle diameter d and between d and $4d$ respectively; D $(H/F)_{min}$ is the corresponding diameter with the minimum value of ratio H/F; U = unstable; S = stable.

Table 2 Properties of tested specimens.

Tested gradation	Tested specimen	Flow direction	Initial dry unit weight after saturation (kN/m^3)	Applied hydraulic gradient (-)	Seepage length (cm)	Test duration (min)	Erosion resistance index at steady state (-)
B	B-V	V	17.36	0.05-0.88	35.0	211	3.8
	B-V rep	V	17.37	0.06-1.30	35.0	210	3.7
	B-H#1	H	17.36	0.05-0.86	35.0	211	4.1
	B-H#2	H	17.37	0.22-3.29	8.1	210	4.0
R3	R3-V	V	18.61	0.06-3.43	35.0	185	4.3
	R3-H	H	18.62	0.09-3.25	35.0	210	4.4
B and R3	B/R3-V	V	17.32 18.67	0.06-3.26	35.0	210	4.6
	B/R3-H	H	17.37 18.64	0.26-2.80	8.1	210	4.0

Table 3 Physical parameters for estimation of I_α.

Tested gradation	*Finer KL* (%)	d_5 (mm)	d_{60} (mm)	d_{90} (mm)	φ (°)	*VBS* (g/100g)	γ_d (kN/m^3)	Estimated value of I_α (-)
B	25	0.11	3.25	3.97	44	0.163	17.37	3.1
R3	25	0.11	3.01	4.48	43	0.110	18.62	3.7

Note: *Finer KL* = percentage of fine based on Kenney and Lau's criterion; d_5, d_{60} and d_{90} are the sieve sizes for which 5%, 60 and 90% respectively of the weighed soil is finer; φ = internal friction angle; *VBS* = blue methylene value; γ_d = dry unit weight; I_α = erosion resistance index.